Available online at www.sciencedirect.com
SCIENCE DIRECT®
Pergamon
Acta Materialia 51 (2003) 4357–4365
Acta MATERIALIA
www.actamat-journals.com

Designing damage-resistant brittle-coating structures: II. Trilayers

Pedro Miranda [a], Antonia Pajares [b], Fernando Guiberteau [a], Yan Deng [c], Hong Zhao [d,1], Brian R. Lawn [d,*]

[a] *Departamento de Electrónica e Ingeniería Electromecánica, Escuela de Ingenierías Industriales, Universidad de Extremadura, 06071 Badajoz, Spain*
[b] *Departamento de Física, Facultad de Ciencias, Universidad de Extremadura, 06071 Badajoz, Spain*
[c] *Department of Materials and Nuclear Engineering, University of Maryland, College Park, MD 20742-2115, USA*
[d] *Department of Materials Science and Engineering, National Institute of Standards and Technology, 100 Bureau Drive, Gaithersburg, MD 20899-8500, USA*

Received 16 January 2003; received in revised form 8 May 2003; accepted 8 May 2003

Abstract

An extension of the FEA-based damage analysis for bilayers in Part I is presented for trilayers consisting of a functional outer layer on an underlying substrate with an intermediate inner core layer. The inner core layer may be used to enhance bonding or load support, but is itself vulnerable to subsurface radial cracking (brittle interlayer) or yield (soft interlayer). A stress analysis is conducted by reducing the trilayer system to an effective bilayer in which the core layer is regarded as either part of the coating or substrate, depending on the damage interface (i.e. outer/inner or inner/substrate). The stress solutions are used to determine generic relations for the critical loads to induce radial cracking or plasticity (or quasiplasticity) in the outer or inner layers, and even in the substrate. A quadratic relationship between critical load and effective coating thickness is preserved; and strength and hardness of the constituent layers remain principal, linearly dependent, material parameters. However, dependence on *relative* outer/inner layer thicknesses and elastic moduli are not generally amenable to exact solution, limiting useful explicit relations to radial cracking in the inner layer. Use of the analysis in constructing design diagrams is again considered.
Published by Elsevier Ltd on behalf of Acta Materialia Inc.

Keywords: Trilayers; Brittle coatings; Cracking; Critical loads; Plasticity

1. Introduction

Following Part I for bilayers, we seek to determine conditions for optimal damage resistance of trilayers with functional outer layers on inner core layers, either brittle or plastic, bonded to a compliant or soft substrate. Such systems are especially representative of dental crowns, where an aesthetic

* Corresponding author. Tel.: +1-301-975-5775; fax: +1-301-975-5012.
E-mail address: brian.lawn@nist.gov (B.R. Lawn).
[1] Present address: Vitreous State Laboratory, Catholic University of America, Washington, DC 20064, USA.

1359-6454/03/$30.00 Published by Elsevier Ltd on behalf of Acta Materialia Inc.
doi:10.1016/S1359-6454(03)00263-5

but weak outer porcelain layer is supported by a stiff inner core layer, either a strong ceramic or hard metal [1–3]—by virtue of load transfer, the core "shields" both the outer porcelain and underlying dentin from the cuspal biting forces [4]. In hip prostheses, acetabular cups are now being fabricated as ceramic/polymer/metal layer structures, with successive components providing improved wear resistance, cushioning and toughness [5]. Trilayers offer the benefits of improved damage resistance and durability without compromising function.

Damage modes in trilayer structures are similar to those in bilayers, except that now the core layer as well as the outer layer and substrate is vulnerable to damage—ceramic cores to fracture [4,6] and metal cores to yield [6,7]. The roles of relative layer thickness and elastic mismatch (as well as other material properties) on stress distributions within the three layers, and the ensuing critical conditions for each damage mode, have yet to be elucidated. Whereas increased elastic mismatch may be expected to enhance damage initiation within any given layer, it may also benefit the structure by ensuring that the damage does not spread to adjacent layers (containment). Accordingly, designing optimal trilayer structures for specific applications requires certain compromises. A sound basis for determining critical conditions for damage initiation is an essential first step in achieving this goal.

Explicit relations for critical loads in terms of the key material and thickness variables are not available for trilayers. We shall build on the bilayer analysis in Part I, again using finite element analysis (FEA), to establish functional dependencies for both ceramic- and metal-based core trilayer systems. For this purpose, it will be convenient to reduce the trilayers to "effective bilayers", regarding the inner support layer as part of either the coating or the substrate, depending on the location of the damage mode. In this way, we can carry over some of the basic relations from Part I. Thus, the quadratic relationship between critical load and effective coating thickness for bilayers is preserved, although the modulus dependence is somewhat more complex. Attention will be paid to whether it is better to use a hard metal or a strong ceramic for the core support layer, a persistent question in the dental crown community. The results will be discussed in the context of the design of trilayers for engineering systems.

2. Stress analysis

2.1. Stress relations

Consider the trilayer system in Fig. 1a, an outer coating layer (o) of thickness d_o and modulus E_o bonded to an inner layer (i) of thickness d_i and modulus E_i, all bonded to a thick substrate (s) of modulus E_s, in contact with a sphere of radius r at load P at the top surface. Following previous experimental observation, subsurface damage initiates adjacent to the interlayer interfaces, along the contact axis. The subsurface modes under consideration here are depicted in Fig. 1a: radial cracking at the bottom surfaces of the inner or outer layer [4]; and yield at the bottom of the outer layer, top or bottom surface of the inner layer, or top surface of the substrate [7]. (As in Part I, we disregard top-surface modes as secondary.) Critical loads can then be evaluated by equating near-interface tensile or von Mises stresses with material strength (cracking) or yield stress (plasticity), respectively.

A principal issue to be examined here is the dependence of the pertinent stresses at the interlayer interfaces on layer thicknesses and moduli. Following Fig. 1, we consider the inner layer as a composite part of either the coating or the substrate, depending on whether the damage mode is located at the o/i or i/s interface. The trilayer is then effectively reduced to a bilayer. Thus, for damage immediately adjacent to the o/i interface (Fig. 1b), the system may be considered as a coating of effective thickness d_o and modulus E_o on a composite substrate of effective modulus $E_s^* = E_i f_s(E_s/E_i, d_o/d_i)$. Such an effective substrate must produce exactly the same stresses in the outer layer of the virtual bilayer as the combined i/s sublayers in the actual trilayer. Then by direct analogy with the bilayer relation Eq. (1) in Part I, the near-interface stresses in the "effective bilayer" have the general form

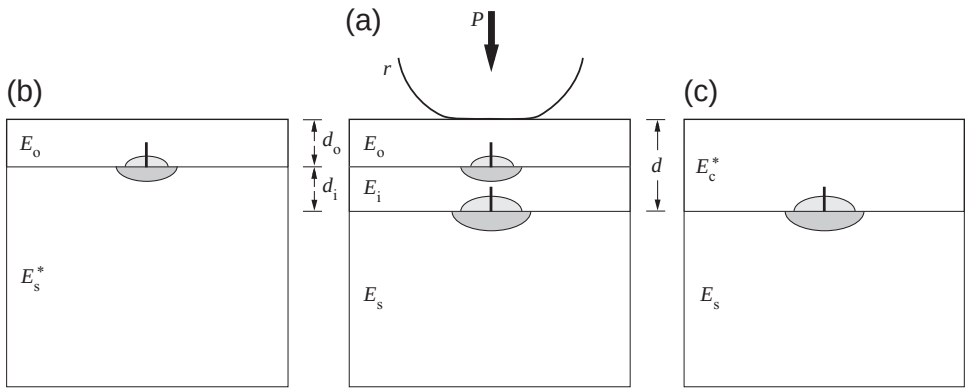

Fig. 1. Schematic of damage in trilayers with outer layer thickness d_o and modulus E_o, inner layer thickness d_i and modulus E_i, on substrate of modulus E_s, from contact at top surface with sphere of radius r at load P. (a) Actual trilayer structure, (b) effective bilayer structure, treating inner layer as part of substrate, (c) effective bilayer structure, treating inner layer as part of coating. Principal subsurface damage modes are radial cracking and yield (shaded) immediately adjacent to outer/inner (o/i) and inner/substrate (i/s) interfaces.

$$\sigma^* = (P/d_o^2)\Sigma^*(E_o/E_s^*) \quad (1a)$$

Similarly, for damage adjacent to the i/s interface (Fig. 1c), the system may be considered as a coating of "effective thickness" $d_o + d_i = d$ and "effective modulus" $E_c^* = E_i f_c(E_o/E_i, d_o/d_i)$ on a substrate of modulus E_s. In this case the near-interface stresses in the effective bilayer may be written

$$\sigma^* = (P/d^2)\Sigma^*(E_c^*/E_s) \quad (1b)$$

Complete evaluation of the effective stresses σ^* in Eq. (1a,b) requires knowledge of the corresponding Σ^* terms for the effective bilayers. These terms may be determined from Eq. (2) in Part I. The effective stresses σ^* in the virtual bilayers may then be converted to equivalent actual stresses σ in the trilayers by invoking the requirement for normal stress and tangential strain compatibility across the layer sections (Appendix A). Then we may propose stress relations analogous to Eq. (1a) for damage adjacent to the o/i interface

$$\sigma = (P/d_o^2)\Sigma(E_o/E_s^*) \quad (2a)$$
$$= (P/d_o^2)\Sigma(E_o/E_i, E_s/E_i, d_o/d_i)$$

and analogous to Eq. (1b) for damage adjacent to the i/s interface

$$\sigma = (P/d^2)\Sigma(E_c^*/E_s) \quad (2b)$$
$$= (P/d^2)\Sigma(E_o/E_i, E_s/E_i, d_o/d_i)$$

In this scheme, an explicit quadratic dependence on layer thickness is retained, but the Σ modulus terms are even more complex than their counterparts in Part I.

2.2. Finite element validation

FEA is carried out as in Part I [4,7] for the system in Fig. 1a. Fig. 2 shows principal normal stresses σ_1 and σ_3 and von Mises shear stresses $\sigma_{13} = \sigma_1 - \sigma_3$ along the contact axis for a representative ceramic/metal/polymer trilayer in Hertzian contact: Young's moduli and Poisson's ratios E_o = 100 GPa and ν_o = 0.22, E_i = 300 GPa and ν_i = 0.33, E_s = 10 GPa and ν_s = 0.35; layer thicknesses d_o = 1 mm = d_i; and sphere radius r = 3.18 mm. Stress distributions are again highly nonlinear across the section, particularly in the outer layer. Discontinuities are once more apparent at the interlayer interfaces, except for σ_3.

In accordance with Eq. (2a,b), Fig. 3 plots FEA-generated o/i stresses σ_1^o, σ_3^o, σ_{13}^o and σ_{13}^i as a function of outer layer thickness quantity d_o^{-2} (Fig. 3a) and i/s stresses σ_1^i, σ_3^i, σ_{13}^i and σ_{13}^s as a function of composite layer thickness d^{-2} (Fig. 3b) for the same material system as in Fig. 2. The FEA data are for thickness ratio d_o/d_i = 1 and fixed sphere radius r = 3.18 mm at contact load P = 25 N. The solid lines are linear best fits to the data at low P.

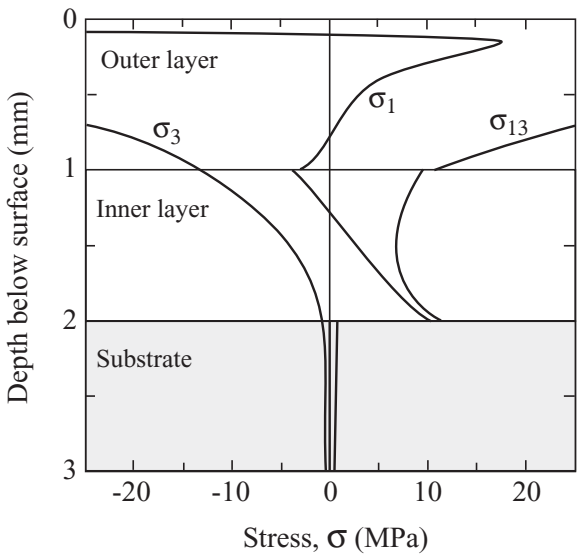

Fig. 2. FEA-generated stresses σ_1, σ_3, and σ_{13} along contact axis, for $d_o/d_i = 1$, $r = 3.18$ mm, for $E_o = 100$ GPa, $E_i = 300$ GPa and $E_s = 10$ GPa ($\nu_o = 0.22$, $\nu_i = 0.33$, $\nu_s = 0.35$). Nonlinear stress distributions across section are again apparent, particularly in outer layer.

Fig. 4 shows plots of σ_1^o versus P/d_o^2 at fixed r/d_o in Fig. 4a (calculated for varying P), and likewise σ_1^i versus P/d^2 at fixed r/d in Fig. 4b, indicating increasing nonlinearities at large P (cf. Fig. 5 in Part I). Figs. 3 and 4 reaffirm the essential inverse quadratic dependence of stress on effective coating thickness for any given material system and near-linearity of this stress with contact load in the asymptotic low-P region.

Fig. 5a plots the quantities $\sigma d_o^2/P = \Sigma$ as functions of E_o/E_i for each o/i stress component, for $E_i = 300$ GPa and $E_s = 10$ GPa ($\nu_o = 0.22$, $\nu_i = 0.30$, $\nu_s = 0.30$) with $d_o = d_i = 1$ mm, in the linear region. Fig. 5b likewise plots $\sigma d^2/P = \Sigma$ as functions of E_i/E_s for each i/s stress component, for $E_o = 100$ GPa and $E_i = 300$ GPa ($\nu_o = 0.22$, $\nu_i = 0.22$, $\nu_s = 0.30$), again with $d_o = d_i = 1$ mm. Note the similarities in these plots with the corresponding plot in Fig. 6 of Part I. The heavy solid line through the σ_1^i FEA data in Fig. 5b is a fit to the transformed i/s equivalent of the σ_1^c stresses in Eq. (2) in Part I, i.e.

$$\sigma_1^i d^2/P = \Sigma_1^i = (1/B)(E_i/E_c^*)\log(CE_c^*/E_s), \quad (1 < E_c^*/E_s < 100) \tag{3}$$

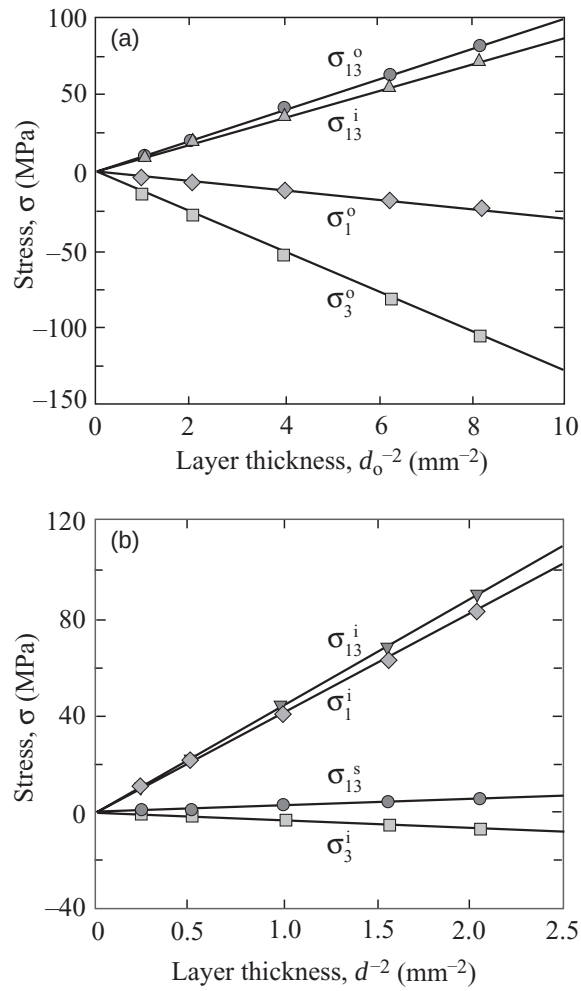

Fig. 3. FEA-generated stresses σ_1, σ_3, and σ_{13} immediately adjacent to (a) o/i interface as a function of d_o^{-2}, and (b) i/s interface as function of d^{-2}, for $d_o/d_i = 1$, $r = 3.18$ mm, $P = 25$ N, $E_o = 100$ GPa, $E_i = 300$ GPa and $E_s = 10$ GPa ($\nu_o = 0.22$, $\nu_i = 0.33$, $\nu_s = 0.35$). Note linear responses over data range.

with $B = 1.35$ and $C = 1.0$ dimensionless coefficients from Part I and $E_c^* = 213$ GPa adjusted to give a best fit. The pre-logarithmic E_i/E_c^* term in Eq. (3) reflects the requirement that the effective coating produce the same stress in the substrate of the virtual bilayer as the combined o/i layers in the actual trilayer (Appendix A). Equations for the actual shear stress components at the i/s interface are more unwieldy and are included in Appendix A. Fits to these equations are represented as soft solid lines in Fig. 5b. Analogous equations for the

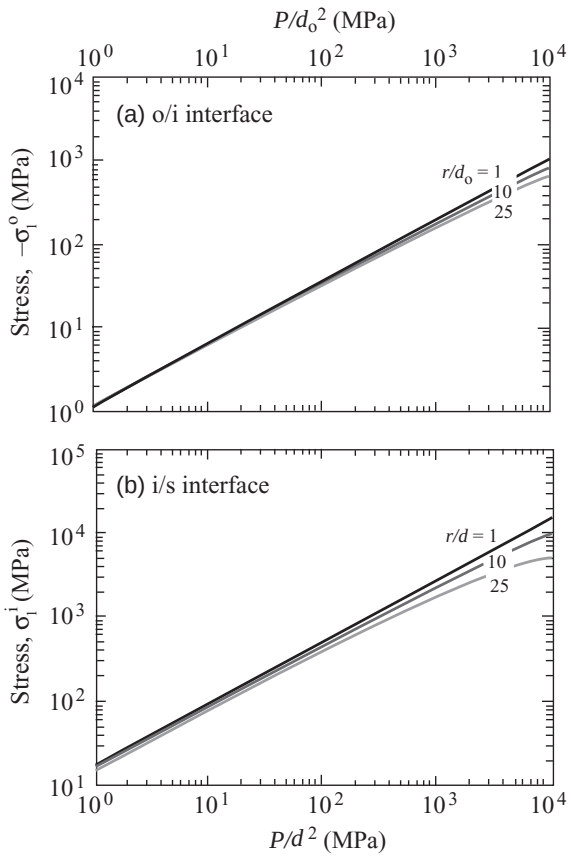

Fig. 4. FEA-generated near-interface stress (a) σ_1^o as function of P/d_o^2 for specified r/d_o values, and (b) σ_1^i as function of P/d^2 for specified r/d values. Plots for d_o/d_i = 1, r = 3.18 mm, P = 25 N, E_o = 100 GPa, E_i = 300 GPa and E_s = 10 GPa (ν_o = 0.22, ν_i = 0.33, ν_s = 0.35). Note nonlinear responses at higher r/d.

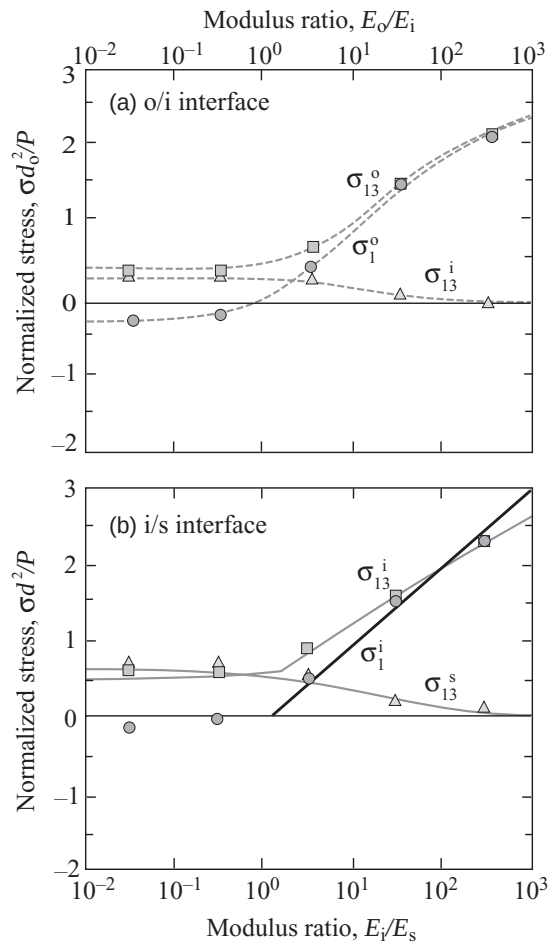

Fig. 5. Stress quantities: (a) $\sigma d_o^2/P$ at o/i interface as function of E_o/E_i, for E_i =300 GPa and E_s = 10 GPa (ν_o = 0.22, ν_i = 0.30, ν_s = 0.30); and (b) $\sigma d^2/P$ at i/s interface as function of E_i/E_s, for E_o = 100 GPa and E_i = 300 GPa (ν_o = 0.22, ν_i = 0.22, ν_s = 0.30). Data points are FEA calculations. In Fig. 5b, heavy line through σ_1 data is best fit to Eq. (3); light lines are fits to shear stress relations in Appendix A. Dashed lines in Fig. 5a are spline fits to the data.

stresses at the o/i interface are subject to greater inaccuracies (recall strong nonlinearities in the outer layers in Fig. 2), and are therefore not included here or in Appendix A. In this case dashed lines in Fig. 5a are simple spline fits through the data points.

Values of relative effective modulus E_c^*/E_i deconvoluted from σ_1^i FEA data for systems with different elastic mismatch and thickness ratios are plotted versus E_o/E_i in Fig. 6a and versus d_o/d in Fig. 6b. Solid lines represent an empirically fitted polynomial function of form similar to the analytical solution for a free-standing bilayer beam or plate in flexural loading [8,9], with adjusted numerical coefficients:

$$E_c^*/E_i = \{1 + \varepsilon^2\delta^3 + \varepsilon\delta(5.66 + 2.18\delta)\} / \{1 + 1.97\delta + \varepsilon\delta[3.69 + 2.18\delta + \delta^2]\} \quad (4)$$

where $\varepsilon = E_o/E_i$ and $\delta = d_o/d_i$. Departures of the effective moduli E^*/E_i from unity increase monotonically with increasing relative outer layer thickness and elastic mismatch.

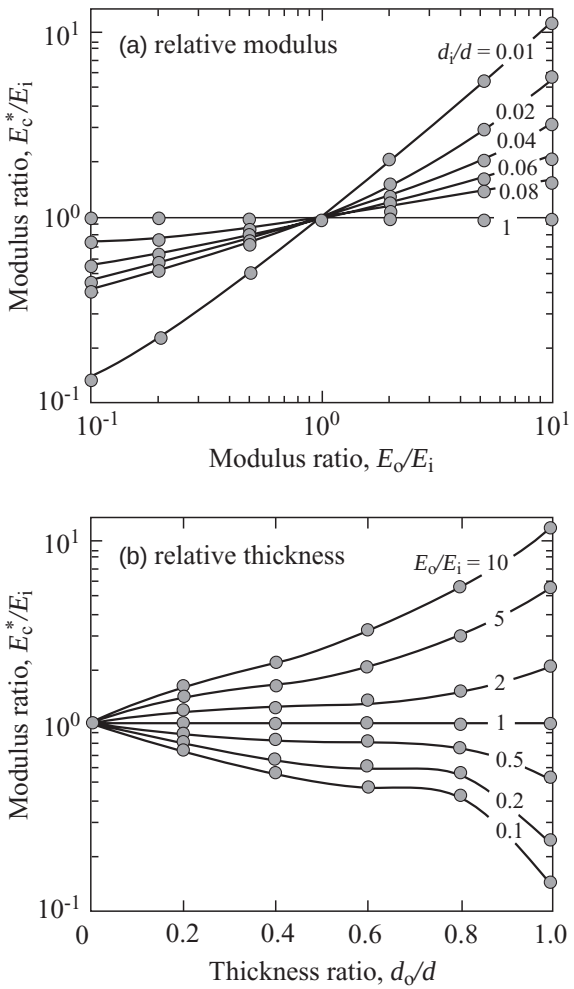

Fig. 6. Relative Young's modulus E_c^*/E_i for effective coating in Fig. 1c, (a) as function of E_o/E_i and (b) as function of d_o/d, calculated here for $d = d_o + d_i = 2$ mm and E_s/E_i=1/700 (ν_o = 0.22, ν_i = 0.22, ν_s = 0.30).

3. Critical loads for damage modes

As in Part I, we impose critical stress criteria to determine threshold load relations for each damage mode depicted in Fig. 1. Thus, suppose damage initiates at a critical stress $\sigma = \sigma_{crit}$ at $P = P_{crit}$ in Eq. (2a,b). Then for the o/i interface

$$P_{crit} = \sigma_{crit} d_o^2 / \Sigma(E_o/E_i, E_s/E_i, d_o/d_i) \quad (5)$$

where σ_{crit} is identified with strength S (tensile stress) or yield stress Y (Mises stress) in the outer and inner layers:

$$P_{crit} = P_R^o, \quad \sigma_{crit} = S_o, \quad \Sigma = \Sigma_1^o \quad (6a)$$

$$P_{crit} = P_Y^o, \quad \sigma_{crit} = Y_o, \quad \Sigma = \Sigma_{13}^o \quad (6b)$$

$$P_{crit} = P_Y^i\uparrow, \quad \sigma_{crit} = Y_i, \quad \Sigma = \Sigma_{13}^i\uparrow \quad (6c)$$

Similarly for the i/s interface

$$P_{crit} = \sigma_{crit} d^2 / \Sigma(E_o/E_i, E_s/E_i, d_o/d_i) \quad (7)$$

where σ_{crit} is now identified with S (tensile stress) or yield stress Y (Mises stress) in the inner and substrate layers:

$$P_{crit} = P_R^i, \quad \sigma_{crit} = S_i, \quad \Sigma = \Sigma_1^i \quad (8a)$$

$$P_{crit} = P_Y^i\downarrow, \quad \sigma_{crit} = Y_i, \quad \Sigma = \Sigma_{13}^i\downarrow \quad (8b)$$

$$P_{crit} = P_Y^s, \quad \sigma_{crit} = Y_s, \quad \Sigma = \Sigma_{13}^s \quad (8c)$$

The arrows are used here to distinguish between yield at the top or bottom inner layer surfaces. In principle, we may now calculate P_{crit} for all six damage modes represented in Eqs. (5)–(8a–c) (Fig. 1), and thus determine which is most likely to precipitate failure in any given trilayer structure.

As in Part I, the hardness relation $H = 3Y$ is a useful adjunct in evaluating the yield stresses in Eqs. (6a–c) and (8a–c).

4. Discussion

We have identified radial cracking and plasticity (or quasiplasticity) modes at outer/inner (o/i) and inner/substrate (i/s) interfaces in trilayer structures. These modes are in addition to the conventional cone cracking and plasticity that may occur at the trilayer top surface in the near-contact region (Part I) [10]. Each damage mode can be an important potential source of ultimate failure: radial cracking is immediately deleterious to strength [10]; and although yield is arguably innocuous in the short term, it can lead to subsequent radial cracking in an outer brittle layer and delamination at the interfaces [11]. By considering the trilayers as effective bilayers in which the inner layer is regarded as either part of the coating or substrate, we have been able to demonstrate that the critical loads for each subsurface damage mode retain explicit linear dependencies on material strength S or yield stress Y (or hardness). The critical loads also remain

quadratically dependent on effective coating layer thickness d_o (o/i interface) or d (i/s interface). However, dependencies on *relative* layer thicknesses d_o/d_i, as well as on elastic moduli E_o/E_i and E_s/E_i, are more complex. For these latter dependencies, we have to resort to numerical evaluation by FEA (Fig. 5). An exception is the critical load for radial cracking in the inner layer, obtainable from Eq. (3) in conjunction with Eq. (8a):

$$P_R^i = BS_i d^2 E_c^*/E_i \log(CE_c^*/E_s), \quad (1 < E_c^*/E_s < 100) \tag{9}$$

In conjunction with Eq. (4) for the effective modulus E_c^*, this is a useful relation for all-brittle coating systems.

In principle, we could construct damage domain diagrams analogous to those calculated from Eq. (6) in Fig. 7 of Part I. However, the addition of an inner core layer substantially increases the number of plots needed for a full description (from 3 to 6), making such diagrams less practical. We limit ourselves here to consideration of damage in the inner core layer. Proper choice of the inner layer material and its relative thickness can "protect" the structure by increasing damage thresholds in adjacent weak-outer and compliant-substrate layers. Such a consideration is particularly relevant to dental crown structures [3] where the core materials tend to be relatively stiff and therefore especially vulnerable to damage associated with flexural stresses from cuspal biting forces [4]. Then comparing Eqs. (6c) and (8a) and Eqs. (8b) and (8a), we may write

$$P_Y^i\uparrow/P_R^i = (Y_i/S_i)(d_o/d)^2(\Sigma_1^i/\Sigma_{13}^i\uparrow) \tag{10a}$$

$$P_Y^i\downarrow/P_R^i = (Y_i/S_i)(\Sigma_1^i/\Sigma_{13}^i\downarrow) \tag{10b}$$

for any fixed coating thickness d. (Analogous relations may be written for competing damage modes in the outer or substrate layers.) If $P_Y^i/P_R^i < 1$, core plasticity occurs first; if > 1, core radial cracking occurs first. Again, the ratio Y/S (or equivalently H/S) emerges a useful brittleness index. Intercomparison of Eqs. (10a) and (10b) enables us to determine whether plasticity is likely to occur first at the upper or lower core surface. In the context of dental crowns, an issue of much current debate is whether it is better to use a metal or ceramic support layer. Eq. (10a,b) confirms that for large Y_i/S_i (ceramics), core radial cracking is the favored damage mode; for small Y_i/S_i (metals), core yield is favored. In the latter case, yield is favored at the upper core surface when d_o/d is small (enhancing the prospect of ensuing radial cracking in the outer layer), and conversely at the lower core surface when d_o/d is large (enhancing the prospect of crown detachment from the underlying dentin). Note that these qualitative assertions may be made without any detailed evaluation of the Σ terms in Eq. (10a,b).

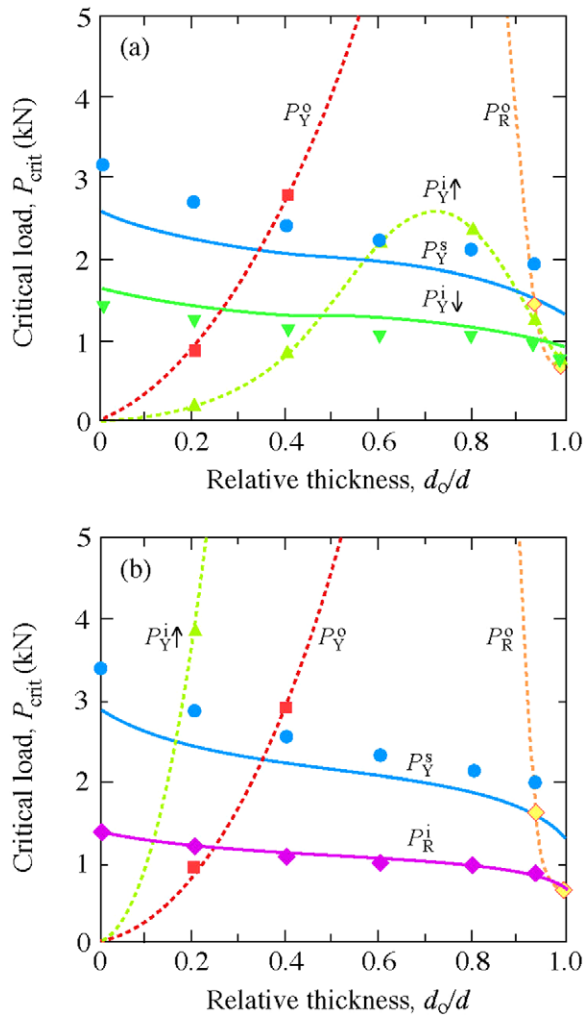

Fig. 7. Design diagram, showing critical loads for (a) porcelain/Co-alloy/dentin and (b) porcelain/alumina/dentin trilayers.

Quantitative predictions of the critical loads P_R^o, P_Y^o, $P_Y^i\uparrow$, P_R^i, $P_Y^i\downarrow$ and P_Y^s in Eqs. (6a–c) and (8a–c) are plotted in Fig. 7 as a function of relative layer thickness d_o/d_i at fixed $d = d_o + d = 1.5$ mm (typical crown thickness) for trilayers with porcelain outer layers and dentin substrates and with (a) Co-alloy and (b) alumina cores, using material parameters from Table 1 of Part I. Data points correspond to evaluations directly from FEA, solid lines through are predictions from Eqs. (4) and (9) for the P_R^i data and from Eq. (4) and Appendix A for the $P_Y^i\downarrow$ and P_Y^s data. Predictions for the o/i modes are omitted for the reasons stated in Section 2.2, and are replaced by dashed line spline fits. P_R^i in Fig. 7a and $P_Y^i\downarrow$ in Fig. 7b lie above the critical load data range. Deviations of the solid lines from the data points may be ascribed to inaccuracies (from fitting procedures and high-load nonlinearities) in the bilayer expressions from Part I used to evaluate the critical load functions. Implicit in the FEA calculations is the assumption that the response remains completely elastic in all materials up to the onset of each damage mode. Strictly, these calculations are valid only up to the onset of first damage, i.e. for the lowest of the curves in Fig. 7. In both systems the predictions indicate transitions in first-damage modes with increasing d_o/d: in the Co-alloy core system (Fig. 7a), top-surface yield in the inner layer at small d_o/d or bottom-surface yield in the inner layer at large d_o/d; in the alumina core system (Fig. 7b), yield in the outer layer at small d_o/d or radial cracking in the inner layer at large d_o/d. (Radial cracking in the outer layer actually becomes dominant in a very small thickness range, $d_o/d > 0.95$.) It would appear that the safest relative thickness region in which to operate is $d_o \approx d_i$. Comparing the two systems, the alumina core is about as susceptible to radial cracking as the Co-alloy is to bottom-surface yield. Thus the key to fabricating superior crowns is to use higher-strength ceramic or harder metal cores, as well as to maintain approximately equal outer and inner layer thicknesses.

Experimental validation of the computational scheme outlined in this study is under way. Relative fatigue susceptibility of the ceramics [12,13] and metals [14] is another factor that warrants further attention in any complete design scheme.

Acknowledgements

This study was supported by internal funds from NIST, and by grants from the US National Institute of Dental and Craniofacial Research (Grant PO1 DE10976), the Junta de Extremadura-Consejeria de Educacion Ciencia y Tecnologia y el Fondo Social Europeo, Spain (Grant IPR00A084) and Secretaria de Estado de Educacion y Universidades, Spain.

Appendix A. Correspondence between effective Σ^* functions and real Σ functions

We may determine real Σ functions in terms of Σ^* functions in Eqs. (1a,b) and (2a,b) by invoking the requirement that the strains at the interfaces are the same in the real trilayer and effective bilayer systems. The i/s terms corresponding to Eq. (2b) are

$$\Sigma_1^i = (E_i/E_c^*)\Sigma_1^{c*} \tag{A.1a}$$

$$\Sigma_3 = \Sigma_3^* \tag{A.1b}$$

$$\Sigma_{13}^i\downarrow = \Sigma_1^i - \Sigma_3 = (E_i/E_c^*)(\Sigma_{13}^{c*} + \Sigma_3^*) - \Sigma_3^* \tag{A.1c}$$

$$\Sigma_{13}^s = \Sigma_{13}^{s*} \tag{A.1d}$$

The Σ^* functions may be determined by analogy with Eq. (2) in Part I, i.e.

$$\Sigma_1^{c*} = (1/B)\log(CE_c^*/E_s), \quad (1 < E_c^*/E_s < 100) \tag{A.2a}$$

$$\Sigma_{13}^{c*} = (1/D)\log(KE_c^*/E_s), (1 < E_c^*/E_s < 1000) = (1/D)\log(K), (E_c^*/E_s < 1) \tag{A.2b}$$

$$\Sigma_{13}^{s*} = 1/G(1 + ME_c^*/E_s) \tag{A.2c}$$

$$\Sigma_3^{c*} = 1/g[1 + m(E_c^*/E_s)^p] \tag{A.2d}$$

with $B = 1.35$, $C = 1.00$, $D = 2.08$, $K = 11.0$, $G = 1.74$, $M = 0.178$, $g = -1.43$, $m = 0.46$ and $p = 0.79$.

Analogous functions for the o/i terms corresponding to Eq. (2a) are subject to considerable inaccuracies, owing to the strong nonlinearities in

the outer layer (see Fig. 2). Accordingly, those functions are not included here.

References

[1] Kelly JR. Ann Rev Mater Sci 1997;27:443.
[2] Kelly JR. J Prosthet Dent 1999;81:652.
[3] Lawn BR, Deng Y, Thompson VP. J Prosthet Dent 2001;86:495.
[4] Miranda P, Pajares A, Guiberteau F, Cumbrera FL, Lawn BR. J Mater Res 2001;16:115.
[5] Willmann G. Adv Eng Mater 2001;3:135.
[6] Lawn BR. Curr Opin Solid State Mater Sci 2002;6:229.
[7] Zhao H, Miranda P, Lawn BR, Hu X. J Mater Res 2002;17:1102.
[8] Chuang T-J, Lee S. J Mater Res 2000;15:2780.
[9] Hsereh C-H, Miranda P. J Mater Res 2003;18:1275.
[10] Lawn BR, Deng Y, Miranda P, Pajares A, Chai H, Kim DK. J Mater Res 2002;17:3019.
[11] Rhee Y-W, Kim H-W, Deng Y, Lawn BR. J Am Ceram Soc 2001;84:1066.
[12] Kim DK, Jung Y-G, Peterson IM, Lawn BR. Acta Mater 1999;47:4711.
[13] Lee C-S, Kim DK, Sanchez J, Miranda P, Pajares A, Lawn BR. J Am Ceram Soc 2002;85:2019.
[14] Suresh S. Fatigue of materials. Cambridge: Cambridge University Press, 1991.